Sea and Sky Infrared Radiances Near the Horizon

Herbert G. Hughes

Naval Ocean Systems Center
San Diego, CA

DTIC
ELECTE
JAN 13 1995
S G D

SWOE Report 89-2
June 1989

Sea and Sky Infrared Radiances Near the Horizon

Herbert G. Hughes

Naval Ocean Systems Center
San Diego, CA

SWOE Report 89-2
June 1989

FOREWORD

SWOE Report 89-2, June 1989, was prepared by Dr. H.G. Hughes of Naval Ocean Systems Center, San Diego, California.

This report is a contribution to the Smart Weapons Operability Enhancement (SWOE) Program. SWOE is a coordinated, Army, Navy, Marine Corps, Air Force and DARPA program initiated to enhance performance of future smart weapon systems through an integrated process of applying knowledge of the broadest possible range of battlefield conditions.

Performance of smart weapons can vary widely, depending on the environment in which the systems operate. Temporal and spatial dynamics significantly impact weapon performance. Testing of developmental weapon systems has been limited to a few selected combinations of targets and environment conditions, primarily because of the high costs of full-scale field tests and limited access to the areas or events for which performance data are required.

Performance predictions are needed for a broad range of background environmental conditions and targets. Meeting this need takes advantage of significant DoD investments by Army, Navy, Marine Corps and Air Force in 1) basic and applied environmental research, data collection, analysis, modeling and rendering capabilities, 2) extensive target measurement capabilities and geometry models, and 3) currently available computational capabilities. The SWOE program takes advantage of these DoD investments to produce an integrated process.

SWOE is developing, validating, and demonstrating the capability of this integrated process to handle complex target and background environment interactions for a world-wide range of battlefield conditions. SWOE is providing the DoD smart weapons and autonomous target recognition (ATR) communities with a validated capability to integrate measurement, information base, modeling and scene rendering techniques for complex environments. The result of a DoD-wide partnership, this effort works in concert with both advanced weapon system developers and major weapon system test and evaluation programs.

The SWOE program started in FY89 under Balanced Technology Initiative (BTI) sponsorship. Present sponsorship is by the U.S. Army Corps of Engineers (lead service), the individual services, and the Joint Test and Evaluation (JT&E) program of the Office of the Director of Defense Research and Engineering (DDR&E), Office of the Secretary of Defense (OSD).

The Program Director is Dr. L.E. Link, Technical Director of the U.S. Army, Cold Regions Research and Engineering Laboratory (CRREL). The Program Manager is Dr. J.P. Welsh, CRREL. The Integration Manager is Mr. Richard Palmer, CRREL. The task areas and their managers are as follows: Modeling Task Area, LTC George G. Koenig, USAF, Geophysics Laboratory (GL), of the Air Force Phillips Laboratories; Information Bases Task Area, Mr. Harold W. West, PE, U.S. Army Engineer, Waterways Experiment Station (WES); Scene Rendering Task Area, Mr. Mike Hardaway, Corps of Engineers, Topographic Engineering Center (TEC); Validation Task Area, Dr. Jon Martin, Atmospheric Sciences Laboratory (ASL) of the Army Materiel Command.

CONTENTS

FIGURES

CONTENTS (Continued)

FIGURES (Continued)

TABLE

INTRODUCTION

The spectral radiance of the sky must be determined in order to predict the performance of passive infrared surveillance systems operating against airborne targets. Spectral radiance is especially important when viewing targets close to the horizon. For these low angles of viewing, the smooth sea is a poor emitter of infrared wavelengths, and its radiance is primarily determined by the emissions of the intervening atmosphere and reflections from the sky. For a wind-ruffled sea, the emissions from the individual wave facets must also be accounted for in the background scene. In the spectral regions about the 6.3-μm water vapor band, where the absorption, and consequently the emissivity, is high, the sky is essentially a blackbody at the temperature of the lowest atmospheric layer, with little variation with elevation angle. In the 8-12-μm region, the absorption (and emissivity) depends on the optical path length, and therefore the radiance will be strongly dependent on the elevation angle. Cloud type and coverage will also have strong effects on radiance, depending upon the elevations and temperatures of the clouds.

In the absence of radiometric measurements, we must presently rely on the LOWTRAN 6 atmospheric transmittance/radiance computer code (Kneizys, et al., 1983), along with measured meteorological parameters and models of aerosol size distributions, to predict the infrared background emissions. The LOWTRAN 6 code has proven to be a versatile tool in predicting atmospheric radiance above the horizon (Hughes and Jensen, 1988). A model has recently been developed of the effective radiance of the sea surface as a function of the viewing zenith angle and sensor height (Wollenweber, 1988b), and has been incorporated into LOWTRAN 6 for processing on an HP-9020 computer. The model (see Appendix A) uses the wave slope statistics of Cox and Munk, 1954, which is based on surface wind speed and direction relative to the look angle. The model is currently limited to the Navy Maritime Aerosol Model (see Appendix B), which in addition to the standard meteorological parameters, requires as inputs the current and 24-hour averaged wind speeds and the origin of the air mass. Basically, the NOSC-developed model calculates the total contributions to radiance at the sensor from the emissions of the intervening atmosphere and the sky reflections and surface emissions from the wave slope surfaces. To-date this model has received very little validation, and the computer code has not yet been made available to the scientific community.

In this report, measurements of near-horizon infrared (8-12-μm) radiances made with a calibrated thermal imaging system are presented. The radiance "scenes" (thermograms) are used to compare the mean equivalent blackbody temperatures corresponding to an area 1 degree above and 1 degree below the horizon during different meteorological and surface-wind-speed conditions. Airborne measurements of the vertical profiles of meteorological parameters and sea surface temperatures are then used to evaluate the ability of the radiance algorithms with the LOWTRAN 6 code to predict the measured results.

MEASUREMENTS

For this study, a Piper Navajo aircraft, equipped with Rosemount temperature and pressure probes and an EG&G dewpoint sensor, made vertical

spirals over the ocean to obtain temperature, relative humidity, and pressure, which are required inputs to the LOWTRAN 6 computer code for calculating the sea and sky radiances. A Barnes PRT-5 radiation thermometer was also onboard the aircraft to measure the actual sea surface temperatures from low-level (<20m), constant-altitude flights. At the time the meteorological parameters were obtained, measurements of infrared (8-12-μm) horizon radiances were also made with a calibrated thermal imaging system (AGA THERMOVISION, Model 780) and a 2.95-degree field-of-view lens.

For these measurements, the scanner was located at an elevation of 33 m on the Point Loma peninsula in San Diego and was directed westward over the ocean. The response of the system is determined by placing a blackbody of known temperature (±0.1°C for temperatures <50°C) in front of the lens aperture. The digitized video signal transfer function of the system then allows the blackbody temperature to be reproduced to within ±0.2°C.

Examples of measured radiance scenes are shown in Fig. 1 and 2 for 25 November and 29 September 1987. The data correspond to low and moderate current wind speeds (V_c) of 2.5 m/s and 7.5 m/s for the respective days. The Thermal Video Processor System (THERMOTEKNIX) available with the AGA system also allows the thermal scene to be displayed in a format consisting of 128 pixel lines (0.023 deg/line). The effective blackbody temperature corresponding to each pixel can then be displayed on the screen by positioning a cursor at the appropriate position. Vertical temperature profiles in the scene are displayed on the right-side of the thermogram as shown in Fig. 1a and 2a. In each case, the horizontal cursor is situated on the pixel corresponding to the maximum temperature (20.4°C or 3.46 mW/cm² sr and 16.5°C or 3.23 mW/cm² sr) which is taken to coincide with the infrared horizon. The increase in temperature with altitude (decreasing zenith angle) in the 29 September scene reflects the increase in air temperature with altitude shown in the Fig. 3. Similarly, the decrease in temperature with altitude in the 25 November scene can be related to the decrease in air temperature with altitude. The larger sky radiance values on 29 September may also partially result from the lower relative humidity above 200 m (Fig. 4), which decreased the number of activated aerosols available to scatter the radiation.

The THERMOTEKNIX system also allows the relative frequency of occurrence of pixels with a specific temperature to be calculated for selected rectangular areas within a scene. When the histogram is plotted, a Gaussian curve (shown with artist-enhanced dots) is calculated which best fits the temperature points. In both the low and moderate wind-speed examples, the sky temperature distributions (Fig. 1b and 2b) are more closely Gaussian than are those of the sea (Fig. 1c and 2c) which show a banded feature. The mean temperature differences for the two examples are 3.6°C and 1.4°C, respectively. In the higher wind speed (9.3 m/s) example shown in Fig. 5 for 19 March 1987, when whitecaps were present, the sea temperature distribution (Fig. 5c) is remarkably similar to a Gaussian distribution. The mean temperature difference between the sky and sea in this case is only 0.2°C. In contrast, the sea and sky mean temperature distributions shown in Fig. 6 during stratus cloud conditions (29 April 1987) were found to be equal, and both were closely Gaussian. The surface wind speed was not measured in this example.

For this study, 18 thermograms recorded during different meteorological and wind-speed conditions in 1987 and 1988 were used to compare the mean cloud-free sky and sea temperatures. In Table 1, the measured mean sky and sea temperatures and the current wind speed are shown. In 12 of the cases, the 24-hour averaged wind speed ($\bar{V}$) and the actual sea surface temperature (T_{ss}) measured by the aircraft were available. Also shown are the combinations of air mass factors (AM) (see Appendix B) and surface visibilities (VIS), which allow the horizon pixel radiance, calculated using LOWTRAN 6 (with the measured profiles of meteorological parameters) to exactly match the measured value (Hughes and Jensen, 1988). For this data set, the mean temperatures were highly correlated (correlation coefficient, r = 0.92), as shown in Fig. 7, with the sea temperature being less than the sky temperature, as indicated by the dashed line for one-to-one correspondence. The mean temperatures differed the most during low wind-speed conditions. As shown in Fig. 8, the differences were found to decrease with increasing wind speed.

CALCULATION OF BACKGROUND SCENES

Earlier work (Hughes and Jensen, 1988) has demonstrated that the sky radiances measured at individual pixel lines within about 1 degree of the horizon can be modeled very closely by using the LOWTRAN 6 code. Figures 9 and 10 show the comparison of the measured and calculated radiances for zenith angles within about 1 degree below the horizon for the scenes in Fig. 1 and 2. In the calculations, the meteorological profiles were divided into 33 layers, as allowed by LOWTRAN 6. The lower layers of the profiles were also divided into sublayers containing the same amount of absorbing and scattering material and the temperature of the original layer. This artificial layering has been found necessary (Wollenweber, 1988a) to remove the anomolous dip (Hughes, 1987) which occurs when aerosols are included in the radiance calculations for zenith angles close to 90 degrees. As the AGA scanner could not be accurately plumbed, the zenith angle of the infrared horizon (the pixel corresponding to the maximum radiance) in each thermogram was taken to be one-half of a pixel less than the angle (θ = 90.179 degrees on 29 September and θ = 90.174 degrees on 25 November) at which the LOWTRAN calculations indicated the refracted ray path first struck the earth. In both cases, the major contributor to the total radiance just below the horizon is the path emission $N(\Theta)_p$. While the reflected sky radiance $N(\Theta)_{rsk}$ and the surface emission $N(\Theta)_{ss}$ are small, their contribution to the total radiance $N(\Theta)_{tot}$ at this low level (33 m) of observation cannot be neglected. It is interesting to note only a small reversal of the relative magnitudes of the reflected sky radiances and surface emissions between the two sets of calculations, which demonstrates the small influence of the wave slopes for the moderate wind speeds on 29 September.

In a similar manner, the mean equivalent blackbody temperatures corresponding to 1-degree areas above and below the horizon were calculated for the 12 cases where vertical profiles of meterological parameters were available. In Fig. 11, the measured and calculated mean sky temperatures, $\overline{T}_m(Sky)$ and $\overline{T}_c(Sky)$, are in close agreement (r = 0.99). In Fig. 12, the calculated mean sea temperatures, $\overline{T}_c(Sea)$, show slightly more variations with the measured values, $\overline{T}_m(Sea)$, but the two are still fairly well correlated (r = 0.90).

DISCUSSION

The demonstrated agreement between the measured and calculated mean temperatures places confidence in the usefulness of the models to calculate radiances as viewed from other altitudes. In a practical sense, the sea radiance model needs to be improved to reduce computer running time. In its present form, approximately 3 minutes of computational time on the HP-9020 are required to calculate the sea radiance at one zenith angle of viewing as compared to approximately 5 seconds for the sky radiance. In this study, approximately 36 minutes of computer time was required to calculate the mean sea temperature within 1 degree of the horizon on each day. The major contributor to the computational time is the myriad of sky-radiance reflections and surface-emission calculations that must be made to account for the radiance from all the wave facets. Computational time could be saved if the surface emissivity and reflectivity calculations were made at a single representative wavelength instead of having to be averaged over a wavelength band for each wave slope. Another way of reducing the computational time is to develop an empirical relationship to directly relate the apparent mean sea temperature to the calculated mean sky temperature.

Inherent in the observed variations between the mean sky and sea temperature differences in Fig. 5 are the surface wind speeds and actual sea surface temperatures. If these parameters are included in a multiple regression analysis for three independent variables, we obtain the following relationship:

$$\overline{T}_m(Sea) = 1.09\ \overline{T}_m(Sky) + 0.37\ V_c + 0.24\ T_{ss} - 10.46 \qquad (1)$$

The correlation coefficient for the multiple regression analysis is 0.97. Only 12 samples were used in the analysis (as compared to 18 samples in the linear regression analysis shown in Fig. 5), which indicates a definite improvement in the correlation when the actual sea surface temperatures and wind speeds are included.

Based on earlier work (Hughes and Jensen, 1988), which demonstrated that the sky radiances measured at individual pixel lines within about 1 degree of the horizon can be modeled very closely by using the LOWTRAN 6 code, and the excellent agreement between the calculated and measured mean sky radiances in Fig. 11, the replacement of $\overline{T}_m(Sky)$ by a calculated value of the mean sky temperature, $\overline{T}_c(Sky)$, would appear justified. This would allow the mean sea temperature to be directly determined by using Eq. 1 and measured profiles of meteorological parameters. Additional data are needed to verify that such a relationship for predicting the apparent mean temperature of the sea is meaningful for other meteorological conditions, sea states, and altitudes of observation. Such a relationship would be a valuable inclusion into a system designer's handbook as a tool for predicting infrared sea backgrounds in locales where only meteorological data are available.

Appendix A

MATHEMATICAL FORMULATION OF SEA RADIANCE MODEL

Consider the atmosphere to be composed of a number, n, of isothermal layers characterized by temperature T_i and transmittance $\tau(\nu,i,\mu)$ along the optical path traversing the ith layer at angle μ, and ν is the spectral wave number. From Kirchoff's law, the radiance of the ith layer is

$$N(\nu,i,\mu)_{sk} = [1 - \tau_a(\nu,i,\mu)]W(T_i)/\pi \tag{A–1}$$

where $\tau_a(\nu,i,\mu)$ is the absorption transmittance and $W(T_i)$ is Planck's blackbody radiation formula. Then the spectral radiance reaching the sea surface through the intervening atmosphere is

$$N(\nu,i,\mu)_{sk}\left[\prod_{j=1}^{i-1}\tau(\nu,j,\mu)\right] = [1 - \tau_a(\nu,i,\mu)]\left[\prod_{j=1}^{i-1}\tau(\nu,j,\mu)\right]W(T_i)/\pi \tag{A–2}$$

Summing the contribution from all layers, the spectral radiance at the sea surface is then

$$N(\nu,\mu)_{sk} = \sum_{i=1}^{i-1}\{[1 - \tau_a(\nu,i,\mu)]\left[\prod_{j=1}^{i-1}\tau(\nu,j,\mu)\right]W(T_i)/\pi\} \tag{A–3}$$

The radiance is allowed to strike a wave facet on the ocean surface with a Gaussian distribution (Cox and Munk, 1954) of angular tilts α and β in the up-wind and cross-wind directions, respectively, so that an amount $N(\nu,\mu)'$ is reflected into the sensor at an altitude H_1 within the mth layer. The probability that radiance hits the facet is equal to the probability that the wave slope exists, i.e.,

$$N(\nu,\mu)' = P(S_x,S_y)N(\nu,\mu)_{sk} \tag{A–4}$$

where

$$P(S_x,S_y) = 1/(2\sigma_x\sigma_y)\mathrm{EXP}[0.05(S_x^2/\sigma_x^2 + S_y^2/\sigma_y^2)] \tag{A–5}$$

and $S_x = \tan\alpha$, $S_y = \tan\beta$, $\sigma_x^2 = 0.003 + 1.92\text{x}10^{3}V_c$, $\sigma_y^2 = 3.16\text{x}103V_c$, with V_c being equal to the current wind speed in the azimuthal direction ϕ with respect to the sensor. Then the total spectral radiance that is reflected from all the wave facets into the line-of-sight of the detector located in the mth layer is

$$N(\nu,\theta)_{rsk} = \left[\prod_{j=1}^{m-1}\tau(j,\theta)\right]\sum_{\mu} R(\nu,\Omega)P(S_x, S_y)N(\nu,\mu)_{rsk} \tag{A–6}$$

where $R(\nu,\Omega)$ is the complex reflectivity of seawater at the reflection angle Ω. In the above equations, both μ and Ω are implicit functions of S_x and S_y given by (Wollenweber, 1988b)

$$\cos\mu = (2S_x/A)\cos\theta'\cos\phi + (2S_y/A)\cos\theta'\cos\phi - (B/A)\sin\theta' \quad \text{(A–7)}$$

$$\cos\Omega = (S_x/A)\cos\theta'\cos\phi) + (S_y/A)\cos\theta'\cos\phi + (1/A)\sin\theta' \quad \text{(A–8)}$$

where $A = S_x^2 + S_y^2 + 1$, $B = S_x^2 + S_y^2 - 1$, and θ' is the sensors' zenith angle at the sea surface reflection point.

In a similar manner, the spectral radiances emitted by the sea surface wave facets (N_{ss}) and the path radiance (N_p) which reach the sensor at the zenith angle θ are given by

$$N(\nu,\theta)_{ss} = \left[\prod_{j=1}^{m-1} \tau(\nu,j,\theta)\right] \sum_{\Omega}^{P} (S_x, S_y)[1 - R(\nu,\Omega)]W(T_{ss})/\pi \quad \text{(A–9)}$$

and

$$N(\nu,\theta)_p = \sum_{i=1}^{m} [1 - \tau_a(\nu,i,\theta)]\left[\prod_{j=i+1}^{m-1} \tau(\nu,j,\theta)\right] W(T_i)/\pi \quad \text{(A–10)}$$

where T_{ss} is the sea surface temperature, and again, the angle μ is implicit in the reflection angle Ω.

Then, the total spectral radiance reaching the detector is the sum of the three components:

$$N(\nu,\theta)_{tot} = N(\nu,\theta)_{rsk} + N(\nu,\theta)_{ss} + N(\nu,\theta)_p \quad \text{(A–11)}$$

The total spectral radiance must then be averaged over the response of the sensor system, which in this case is taken to be the 8- to 12-μm wavelength band. Subroutines have been introduced into LOWTRAN 6 (Wollenweber, 1988b) to calculate the band-averaged radiance. The reflection and zenith angles are calculated with Eq. A–5, A–7, and A–8, corresponding to the incremented values of wave slopes in the intervals $-3\sigma_{x,y} < S_{x,y} < 3\sigma_{x,y}$.

Appendix B

DESCRIPTION OF THE LOWTRAN 6 NAVY MARITIME AEROSOL MODEL

The particle size distribution model (at radius r) is the sum of three log-normal distributions given by

$$n(r) = \sum_{i=1}^{3} A_i \exp[-(\ln \frac{r}{fr_i})^2] \quad (\text{cm}^{-3} \bullet \mu\text{m}^{-1}) \tag{B-1}$$

where

$$A_1 = 2000(AM)^2 \tag{B-2}$$

$$A_2 = 5.866(\overline{V} - 2.2) \tag{B-3}$$

$$A_3 = 10\ (0.06V_c - 2.8) \tag{B-4}$$

Component A_1 represents the contribution by continental aerosols. AM is an air mass parameter that is allowed to range between integer values of 1 for open ocean and 10 for coastal areas and is given by

$$AM = INT(Rn/4) + 1 \tag{B-5}$$

where Rn is the measured atmospheric radon content expressed in pCi/m^3. In the absence of radon measurements, the air mass factor can be related to the elapsed time, T(days), for the air mass to reach the point of observation:

$$AM = INT[9\exp(-T/4)] + 1 \tag{B-6}$$

Components A_2 and A_3 represent equilibrium sea spray particles generated by the surface wind speed averaged over 24 hours ($\overline{V}$, in m/s) and the current surface wind speed (V_c, in m/s), respectively. (It should be noted that the current wind speed component is different from the value published in LOWTRAN 6. This modification was found to be necessary in order to match previously published measurements of infrared sky radiances and near-surface aerosol size distributions (Hughes, 1987)). In Eq. B–1, r_i , the modal radius for each component referenced to a relative humidity of 80% (r_1 = 0.03 μm, r_2 = 0.24 μm, and r_3 = 2.0 μm), is allowed to grow with relative humidity (RH) according to the formula (Fitzgerald, 1975)

$$f = [(2 - RH/100)/6(1 - RH/100)]^{1/3} \tag{B-7}$$

The contribution to the total extinction or absorption by each component can then be written as

$$\sigma_{e,a}\ (\lambda)_i = (SF)\{C_i \int_r Q_{e,a}(\lambda,r,m)\exp[-(\ln \frac{r}{fr_i})^2]r^2 dr\} \tag{B-8}$$

where $C_i = (0.001\pi/f)A_i$.

The factor f^{-1} in the expression for C_i ensures a constant total number of particles as the relative humidity increases. $Q_{e,a}$ (λ,r,m) is the cross-section for either the extinction or absorption normalized to the geometrical cross-section of the spherical particle, and m is the complex refractive index, which is allowed to change from that of dry sea salt as the particle deliquesces with increasing humidity. LOWTRAN 6 provides precalculated values in tabular form of the parameter $\sigma_{e,a}$ $(\lambda_i)/C_i$ at discrete wavelengths for four relative humidities (50%, 85%, 90%, and 99%), from which the average extinction for a specific wavelength band and relative humidity can be readily determined by interpolation. When an observed surface visibility (VIS_o) is available as an input to the model, the amplitudes of the three components are adjusted by a scaling factor (SF) so that the calculated aerosol extinction coefficient, σ_c, at a wavelength of 0.55 μm is the same as the observed extinction, σ_o, determined from the relationship

$$VIS_o = \frac{3.912}{\sigma_o + \sigma_r} \tag{B–9}$$

where σ_r is the Rayleigh contribution to extinction at 0.55mm.

REFERENCES

Cox, C. and W. Munk, "Measurements of Roughness of the Sea Surface from Photographs of the Sun's Glitter," Jour. Opt. Soc. of Am., 44, 838 (1954).

Fitzgerald, J. W., "Approximate Formulas for the Equilibrium Size of an Aerosol Particle as a Function of its Dry Size and Composition and the Ambient Relative Humidity," J. Appl. Meteorol., 14, 1044 (1975).

Hughes, H. G., "Evaluation of the LOWTRAN 6 Navy Maritime Aerosol Model Using 8 to 12 μm Sky Radiances," Opt. Eng., 26, 1155 (1987).

Hughes, H. G. and D. R. Jensen, "Aerosol Model Selection Using Surface Measurements of IR Horizon Radiances and Satellite Detected Visible Radiances," Appl. Opt., 27, 4367 (1988).

Kneizys, F. X., E. P. Shettle, W. O. Gallery, J. H. Chetwynd, Jr., J. H. Abreu, J. E. A. Selby, S. A. Clough and R. W. Fenn, "Atmospheric Transmittance/Radiance: Computer Code LOWTRAN 6," Air Force Geophysical Laboratory Technical Report No. 83-0187, August 1983.

Wollenweber, F. G., "Effects of Atmospheric Model Layering on LOWTRAN 6 Calculations of 8 to 12 μm Near Horizon Sky Radiance," NOSC TD 1193, January 1988a.

———, "Infrared Sea Radiance Modeling Using LOWTRAN 6," NOSC TD 1355, September 1988b.

LIST OF CAPTIONS

Figure 1. Thermograms of near-horizon infrared radiances on 25 November 1987 during low wind speed conditions (2.5 m/s). (a) Vertical profile of effective blackbody temperature near the horizon, and temperature histograms corresponding to areas 1 degree above (b) and 1 degree below (c) the horizon. In each histogram a Gaussian curve is displayed as a series of dots which best fit the temperature points.

Figure 2. Thermograms of near-horizon infrared radiances on 29 September 1987 during moderate wind speed conditions (7.5 m/s) without the presence of whitecaps. (a) Vertical profile of effective blackbody temperature near the horizon, and temperature histograms corresponding to areas 1 degree above (b) and 1 degree below (c) the horizon. In each histogram a Gaussian curve is displayed as a series of dots which best fit the temperature points.

Figure 3. Profiles of air temperature measured with altitude on 29 September and 25 November 1987 off the coast of San Diego, California.

Figure 4. Profiles of relative humidity measured with altitude on 29 September and 25 November 1987 off the coast of San Diego, California.

Figure 5. Thermograms of near-horizon infrared radiances on 19 March 1987 during moderate wind speed conditions (9.2 m/s) when whitecaps were present. (a) Vertical profile of effective blackbody temperature near the horizon, and temperature histograms corresponding to areas 1 degree above (b) and 1 degree below (c) the horizon. In each histogram a Gaussian curve is displayed as a series of dots which best fit the temperature points.

Figure 6. Thermograms of near-horizon infrared radiances on 29 April 1987 during stratus cloud conditions (wind speed not measured). (a) Vertical profile of effective blackbody temperature near the horizon, and temperature histograms corresponding to areas 1 degree above (b) and 1 degree below (c) the horizon. In each histogram a Gaussian curve is displayed as a series of dots which best fit the temperature points.

Figure 7. Regression analysis of measured mean sky temperatures, $\overline{T}_m(Sky)$, and mean sea temperatures, $\overline{T}_m(Sea)$. The dashed line corresponds to a one-to-one correspondence between the two parameters.

Figure 8. Regression analysis of the difference between the measured mean sky temperatures, $\overline{T}_m(Sky)$, and mean sea temperatures, $\overline{T}_m(Sea)$, and the surface wind speed.

Figure 9. Comparison of the measured and calculated IR radiances for zenith angles about 1 degree below the horizon on 25 November 1987.

Figure 10. Comparison of the measured and calculated IR radiances for zenith angles about 1 degree below the horizon on 29 September 1987.

Figure 11. Correlation between the measured, $\overline{T}_m(Sky)$, and calculated, $\overline{T}_c(Sky)$, mean sky temperatures.

Figure 12. Correlation between the measured, $\overline{T}_m(Sea)$, and calculated, $\overline{T}_c(Sea)$, mean sea temperatures.

25 Nov 1987
(V_c = 2.5 m/s)

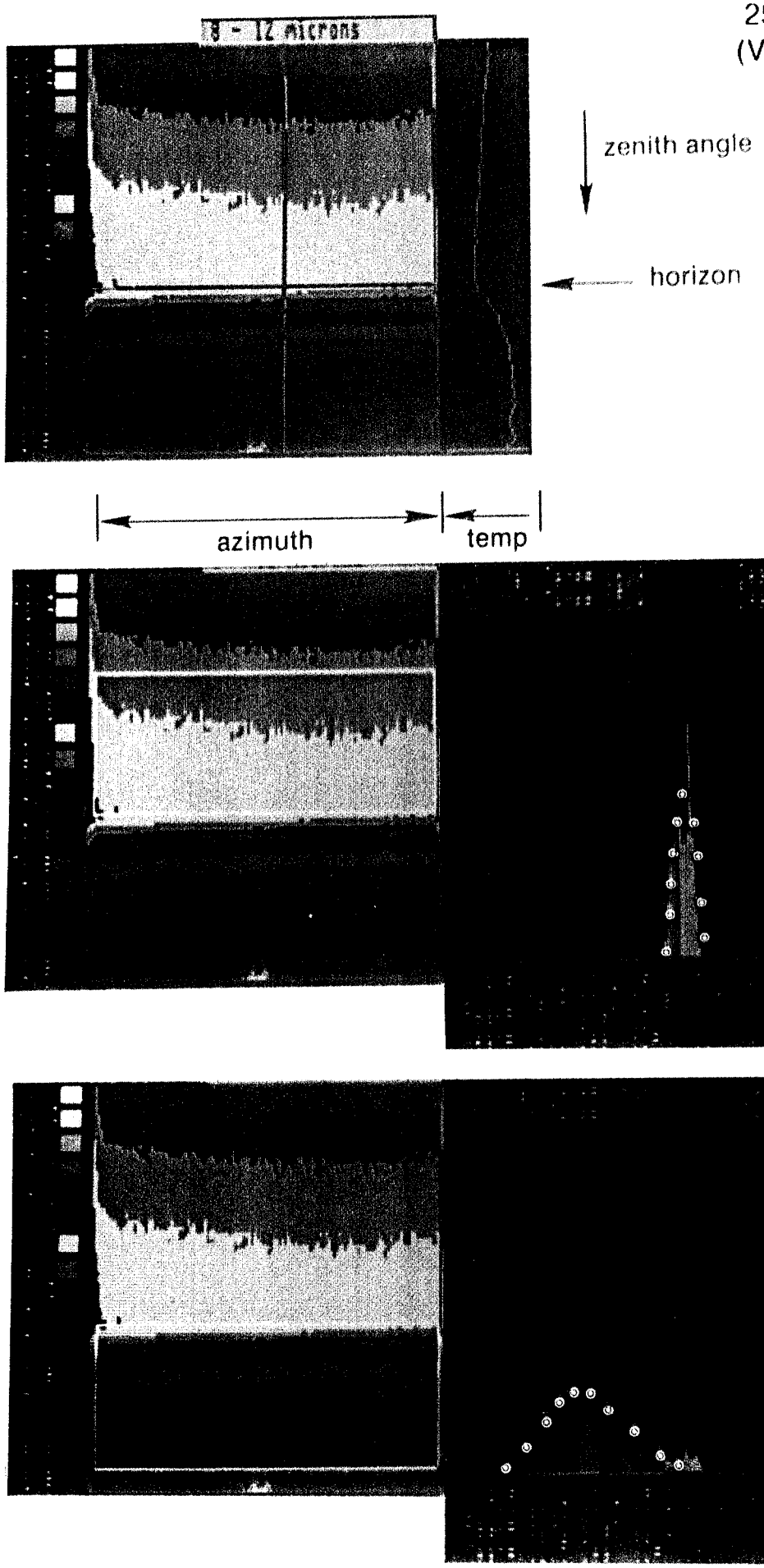

FIGURE 1

29 Sep 1987
(V_c = 7.5 m/s)

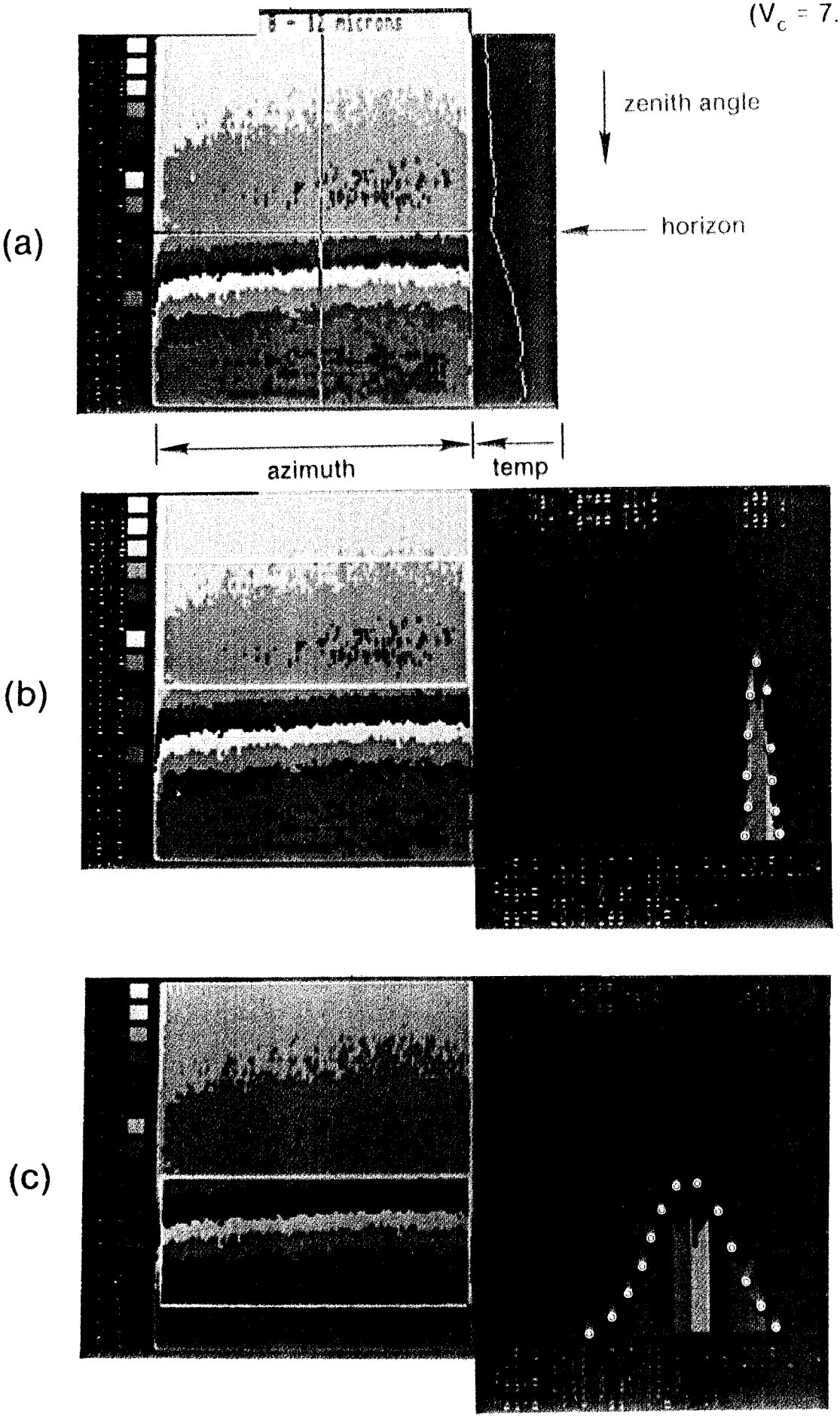

FIGURE 2

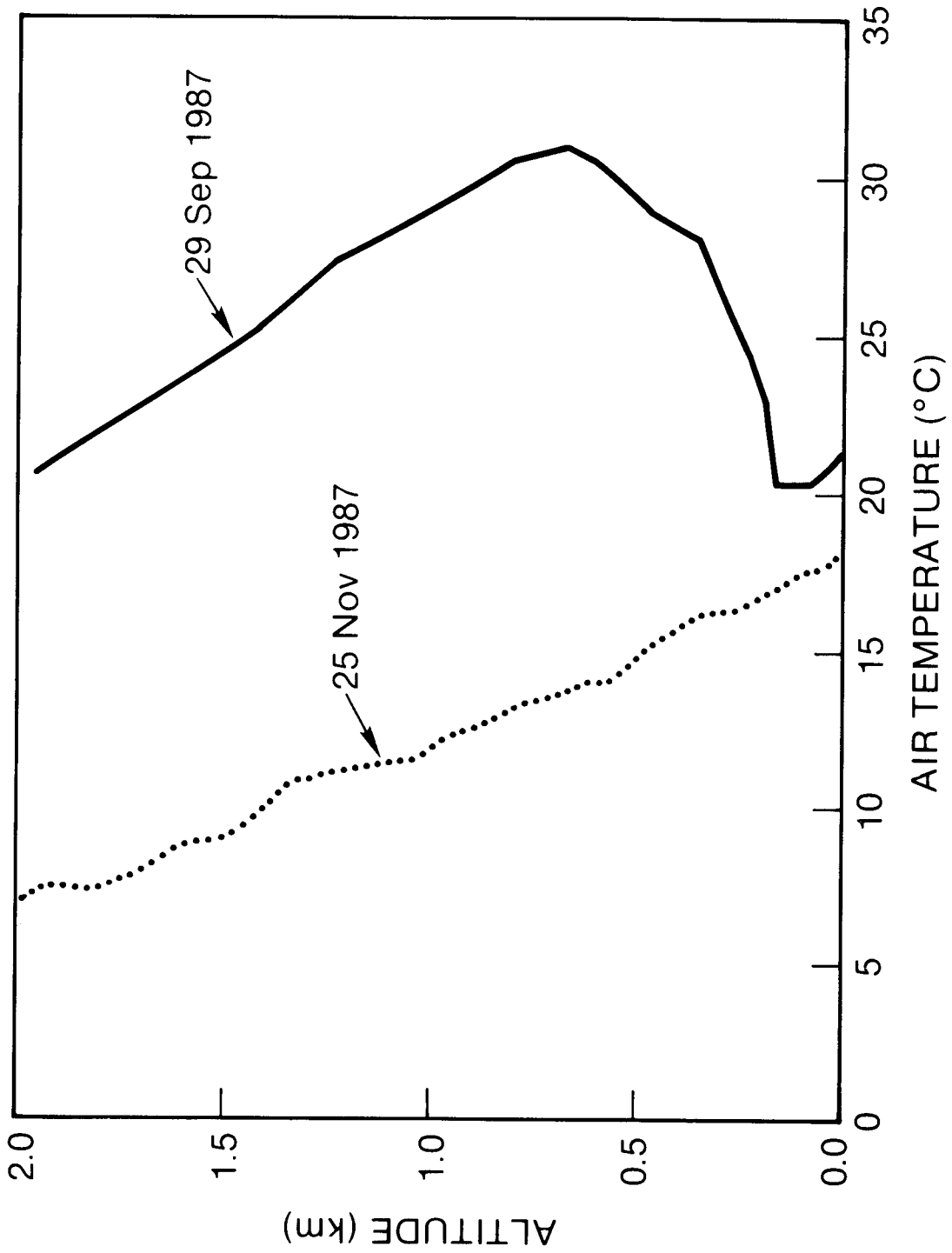
29 Sep 1987
25 Nov 1987
ALTITUDE (km)
2.0
1.5
1.0
0.5
0.0
0
5
10
15
20
25
30
35
AIR TEMPERATURE (°C)

FIGURE 3

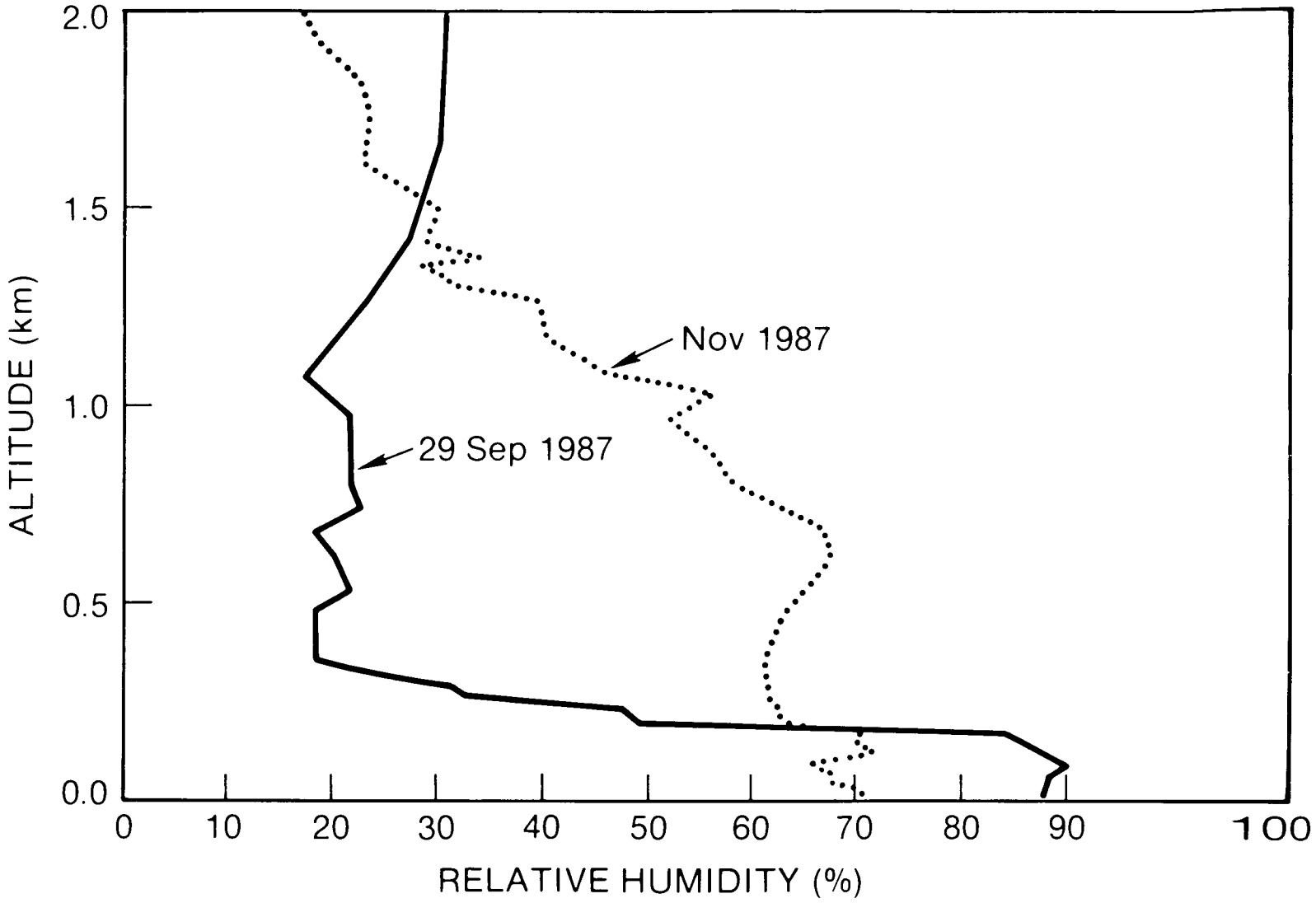
2.0
1.5
1.0
0.5
0.0
ALTITUDE (km)
Nov 1987
29 Sep 1987
0
10
20
30
40
50
60
70
80
90
100
RELATIVE HUMIDITY (%)

19 Mar 1987
(V_c = 9.3 m/s)

(a)

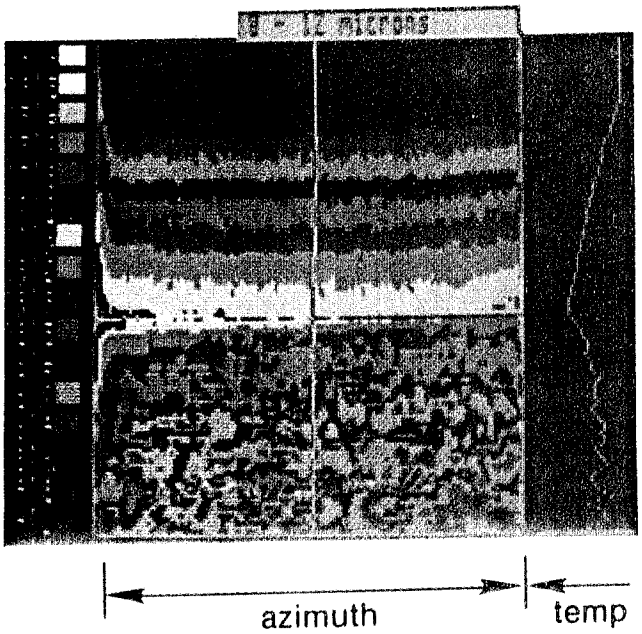

(b)

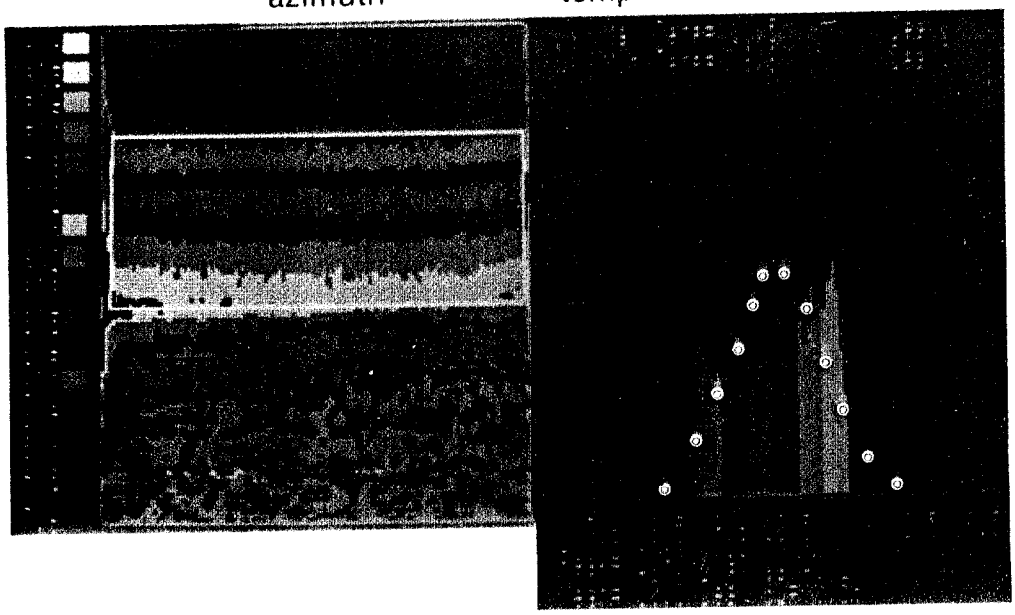

(c)

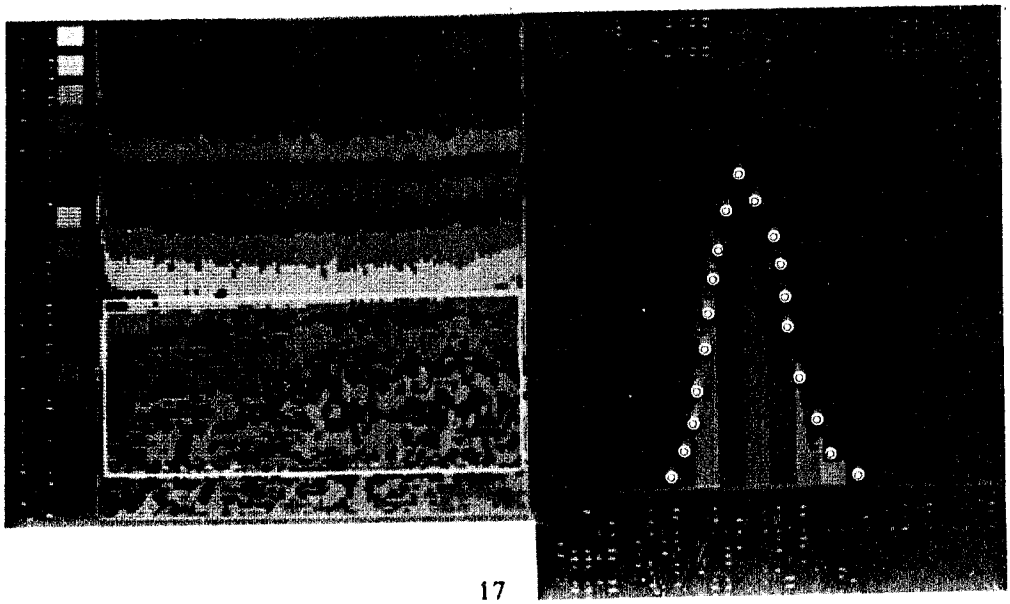

FIGURE 5

29 Apr 1987
(Stratus)

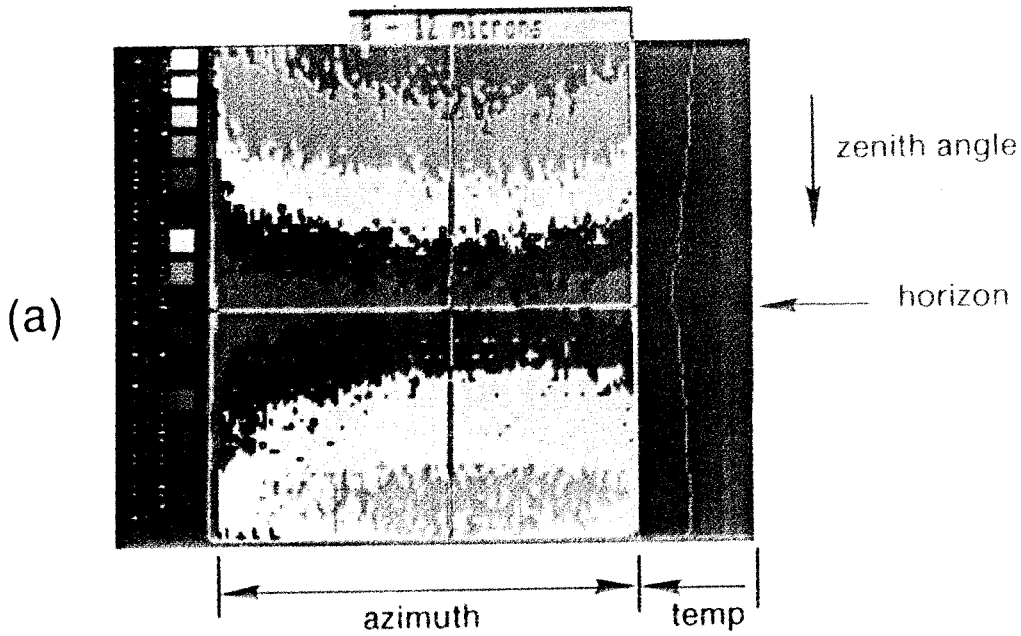

(a)

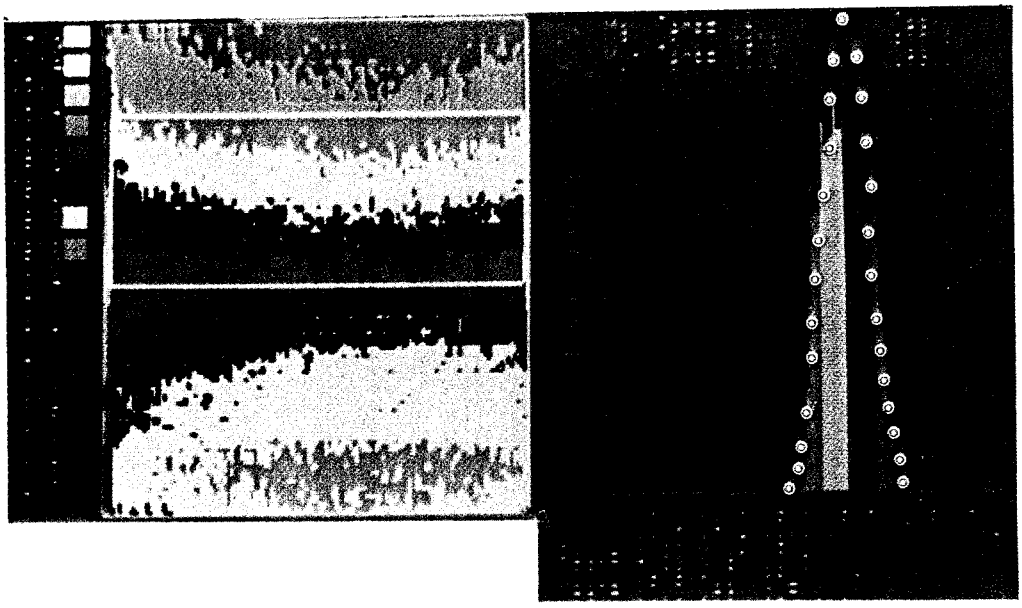

(b)

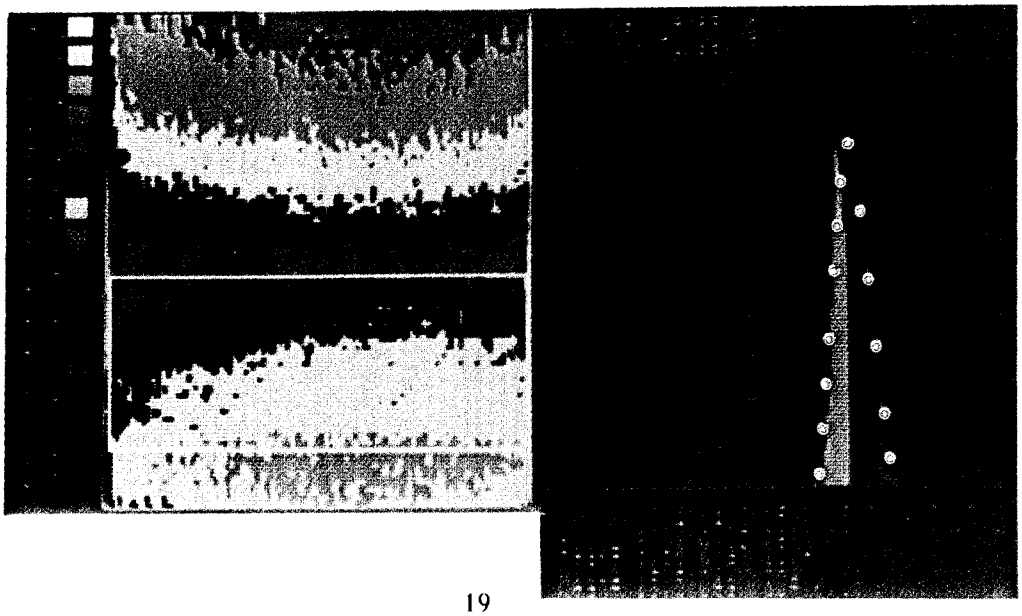

(c)

FIGURE 6

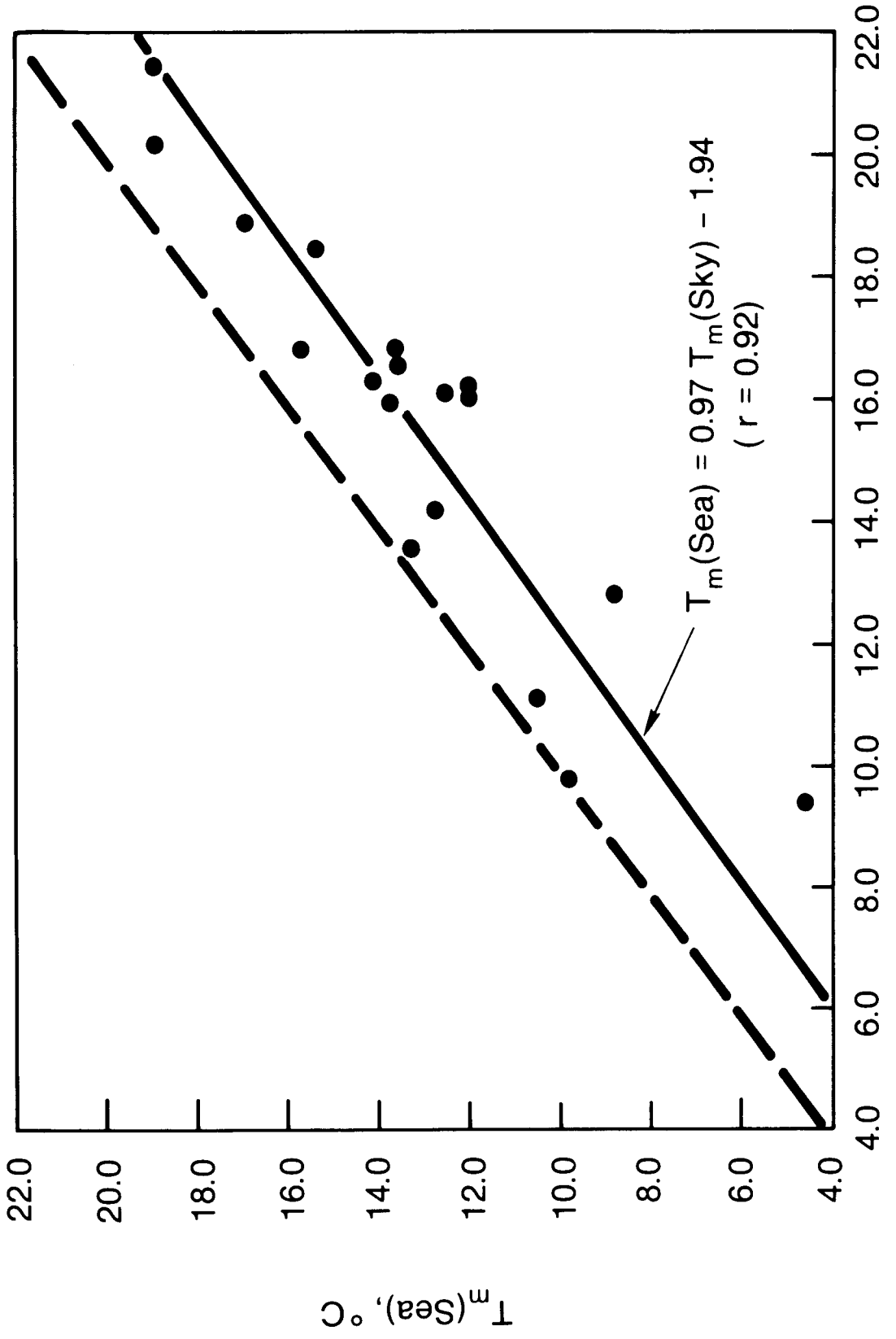
T_m(Sea) = 0.97 T_m(Sky) – 1.94
(r = 0.92)
T_m(Sea), °C
T_m(Sky), °C
22.0
20.0
18.0
16.0
14.0
12.0
10.0
8.0
6.0
4.0

FIGURE 7

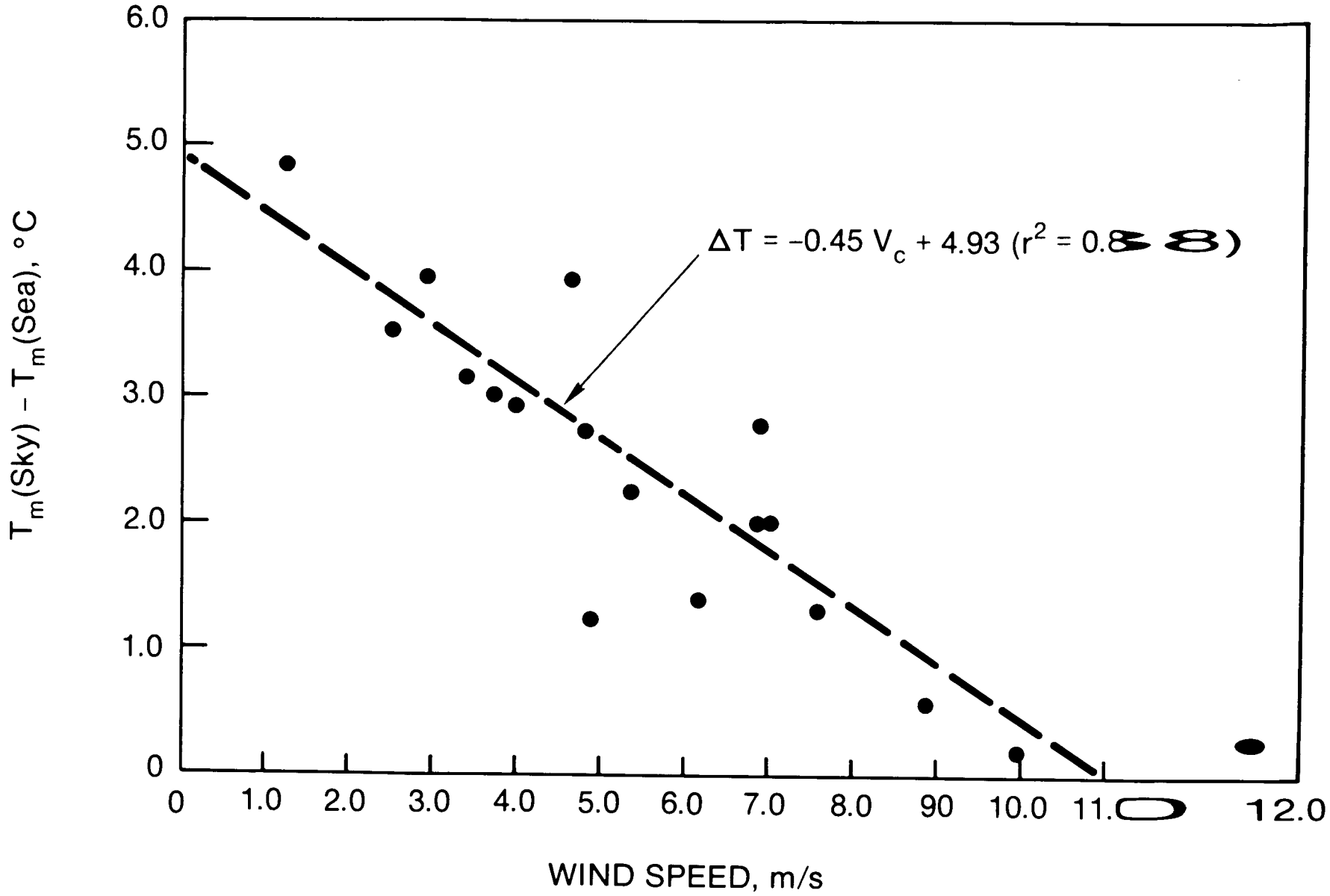
6.0
5.0
4.0
3.0
2.0
1.0
0
$T_m(Sky) - T_m(Sea)$, °C
$\Delta T = -0.45\ V_c + 4.93\ (r^2 = 0.88)$
0
1.0
2.0
3.0
4.0
5.0
6.0
7.0
8.0
9.0
10.0
11.0
12.0
WIND SPEED, m/s

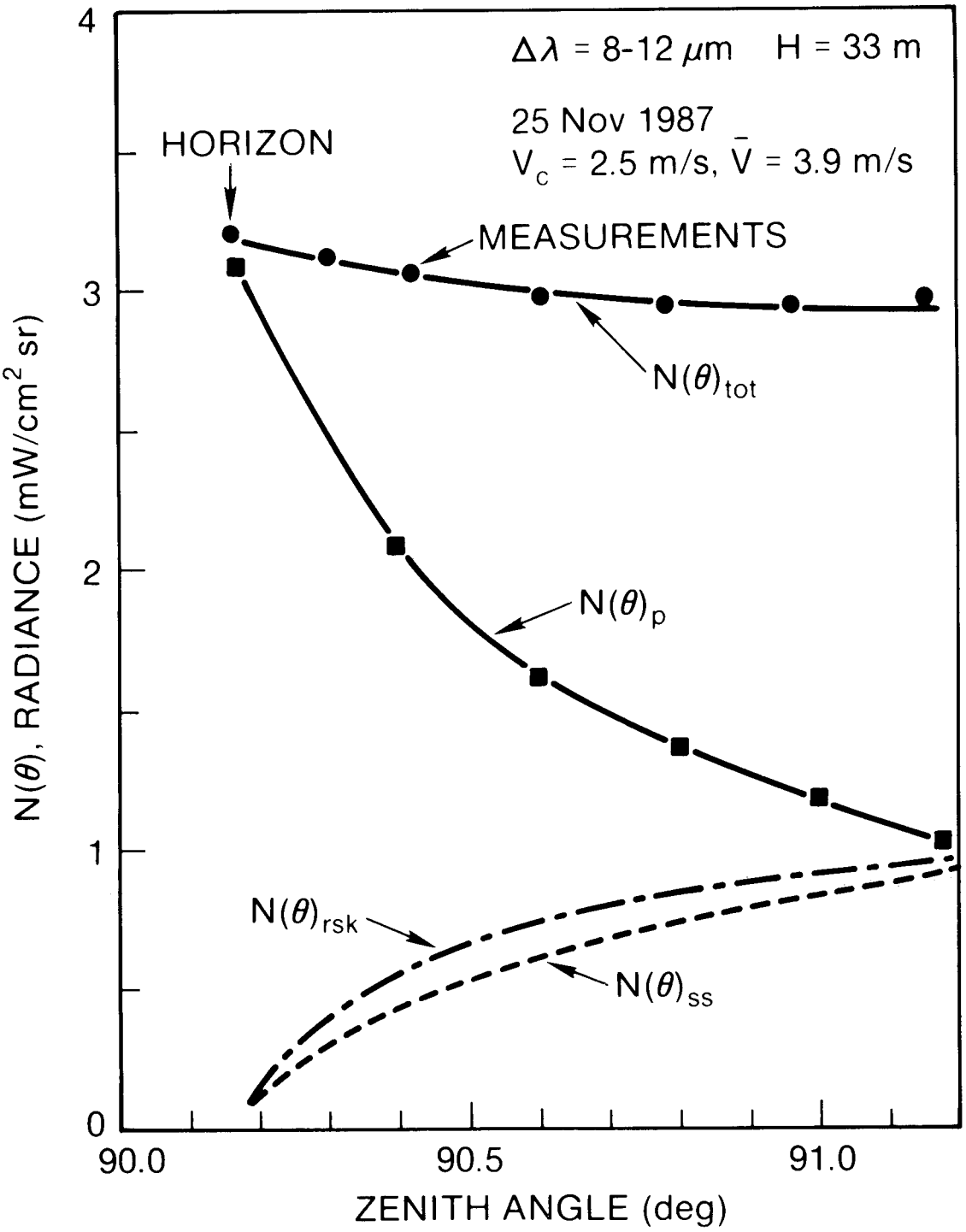
Δλ = 8-12 μm H = 33 m
25 Nov 1987
V_c = 2.5 m/s, V̄ = 3.9 m/s
HORIZON
MEASUREMENTS
N(θ)_tot
N(θ)_p
N(θ)_rsk
N(θ)_ss
N(θ), RADIANCE (mW/cm² sr)
ZENITH ANGLE (deg)
0
1
2
3
4
90.0
90.5
91.0

FIGURE 9

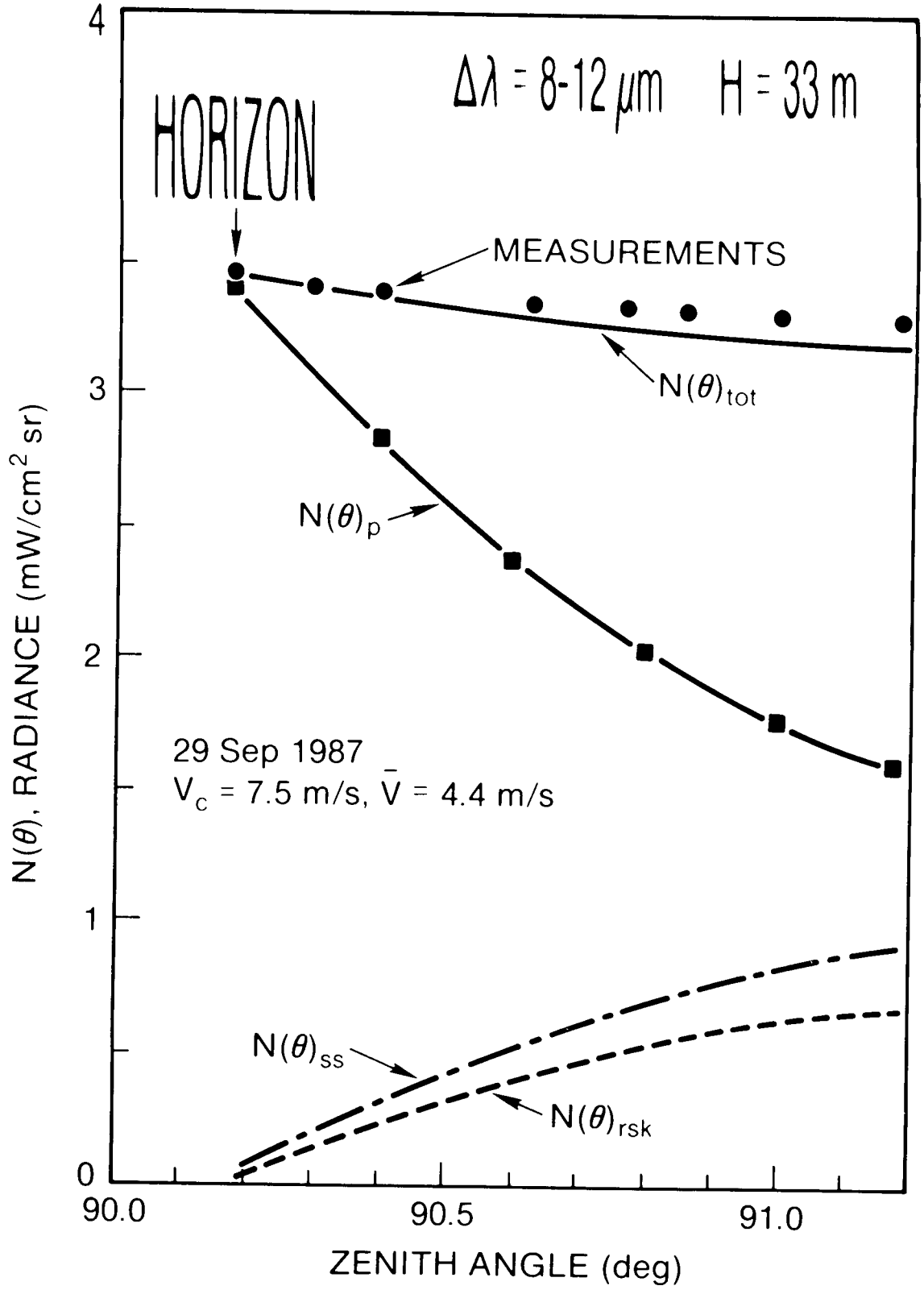
HORIZON
Δλ = 8-12 μm H = 33 m
MEASUREMENTS
N(θ)tot
N(θ)p
N(θ)ss
N(θ)rsk
29 Sep 1987
Vc = 7.5 m/s, V̄ = 4.4 m/s
N(θ), RADIANCE (mW/cm2 sr)
ZENITH ANGLE (deg)
0
1
2
3
4
90.0
90.5
91.0

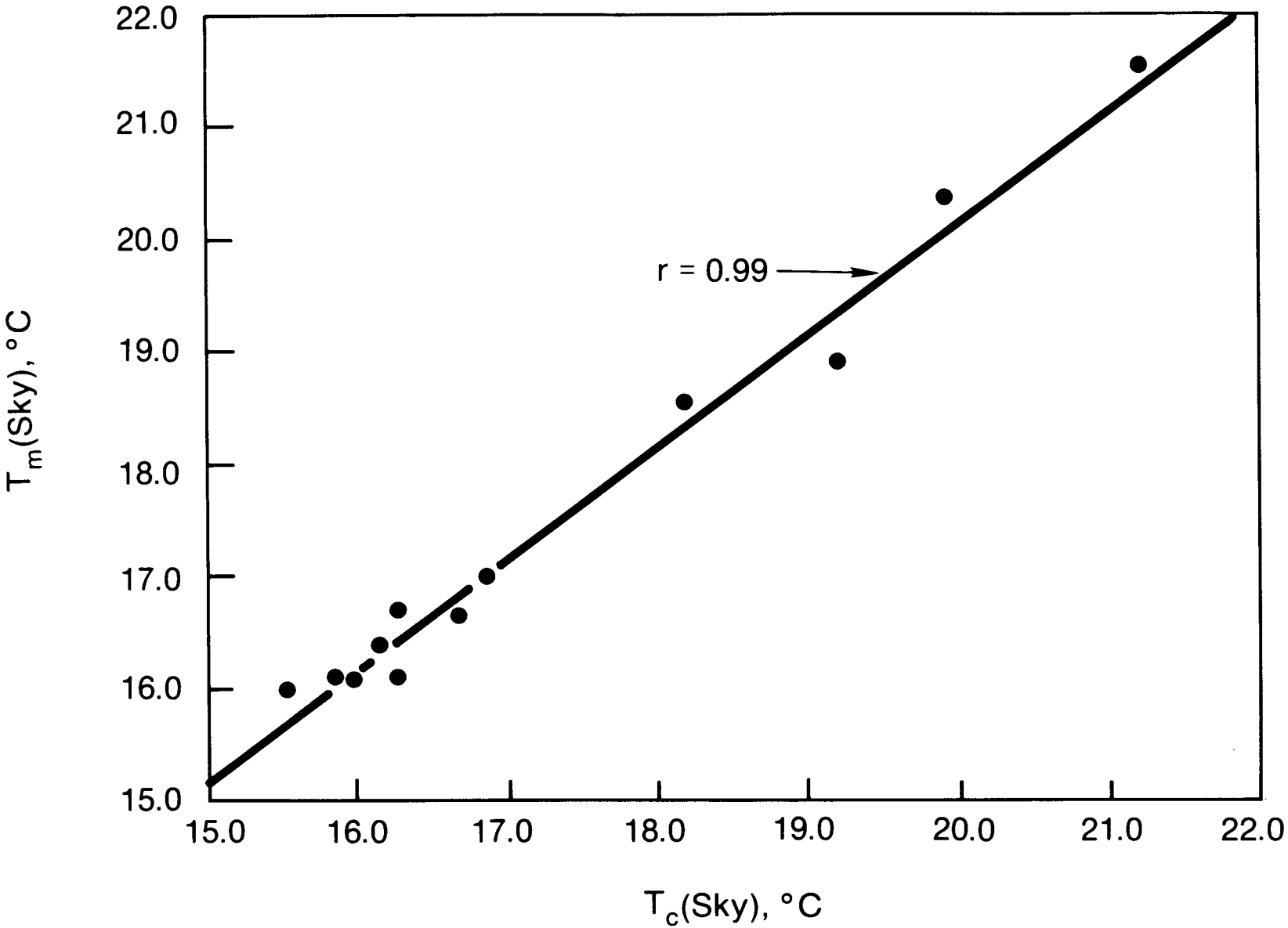
22.0
21.0
20.0
19.0
18.0
17.0
16.0
15.0
r = 0.99
T_m(Sky), °C
15.0
16.0
17.0
18.0
19.0
20.0
21.0
22.0
T_c(Sky), °C

FIGURE 11

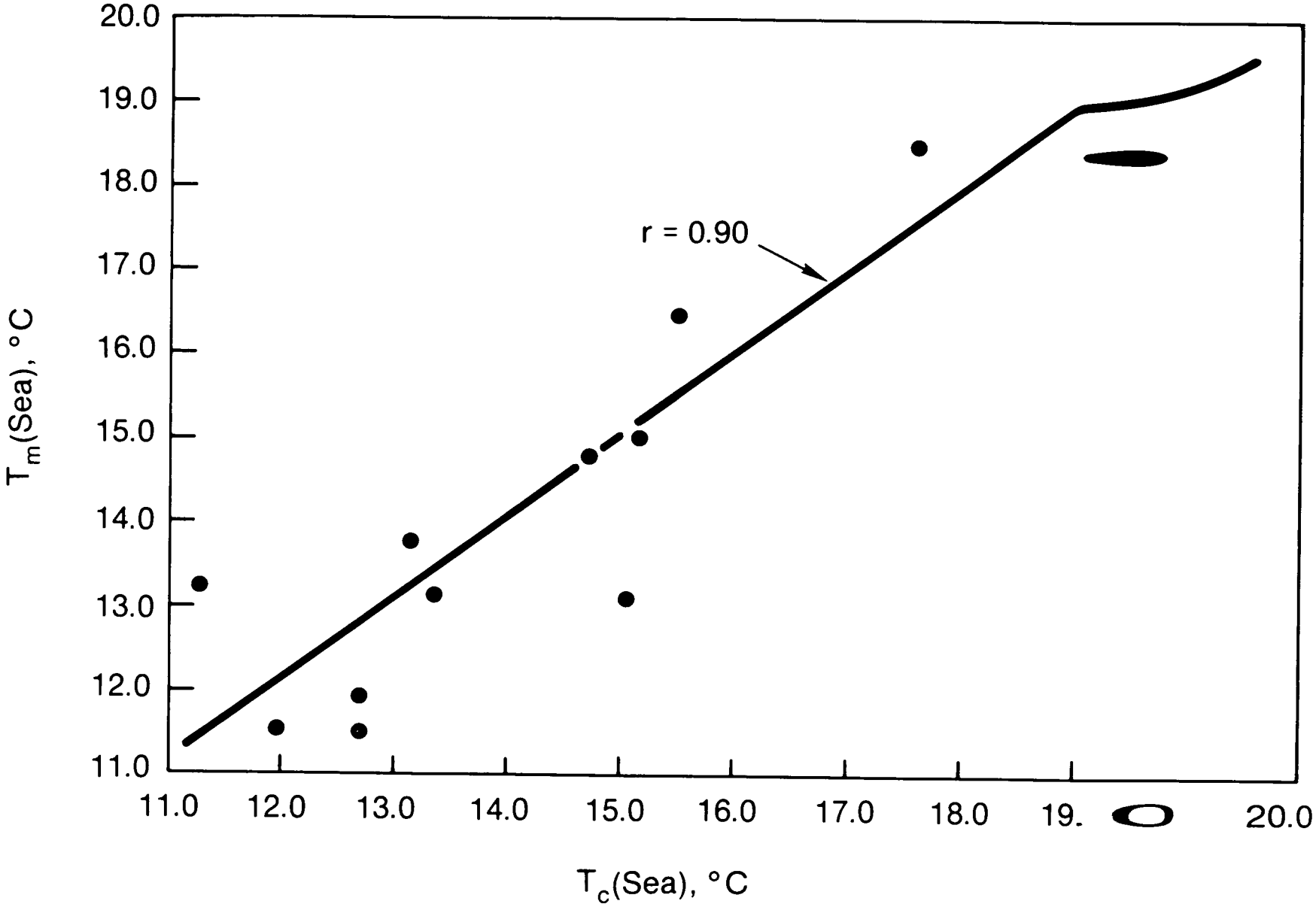
20.0
19.0
18.0
17.0
16.0
15.0
14.0
13.0
12.0
11.0
r = 0.90
T_m(Sea), °C
11.0
12.0
13.0
14.0
15.0
16.0
17.0
18.0
19.
20.0
T_c(Sea), °C

TABLE 1. Mean sky, $\overline{T}_m(Sky)$, and sea, $\overline{T}_m(Sea)$, temperatures, current wind speed, V_c, 24-hour averaged wind speed, $\overline{V}$, and the actual sea surface temperature, T_{ss}, measured on the days indicated. VIS and AM are the inferred visibility and air mass factor, respectively.

Date	$\overline{T}_m$(Sky) (°C)	$\overline{T}_m$(Sea) (°C)	V_c (m/s)	$\overline{V}$ (m/s)	T_{ss} (°C)	VIS (km)	AM
(1987) 19 Mar	10.1	9.9	9.3				
25 Mar	9.5	4.6	1.5				
26 Mar	12.9	8.9	4.1				
3 Apr	11.2	10.5	8.8				
18 May	14.3	12.8	6.1				
26 May	13.6	13.3	11.6				
30 Jun	16.4	14.3	6.8	5.0	17.8	45.0	4
8 Sep	21.6	18.8	4.7	2.6	18.7	16.5	3
17 Sep	19.0	16.9	6.9	2.9	18.1	31.5	5
29 Sep	20.3	18.9	7.5	4.4	15.2	26.5	4
3 Nov	16.0	13.7	5.3	3.9	17.7	24.6	4
12 Nov	18.6	15.4	3.2	2.7	17.0	24.5	3
24 Nov	16.7	13.8	6.8	3.4	17.4	18.0	6
25 Nov	16.1	12.5	2.5	3.9	17.6	21.0	4
(1988) 9 Jun	16.1	12.1	2.9	2.8	16.4	37.0	3
10 Jun	16.1	12.1	4.6	2.2	16.8	35.5	4
9 Nov	16.7	13.6	3.7	2.1	19.3	41.3	2
10 Nov	17.0	15.6	4.8	2.8	20.3	45.8	2

REPORT DOCUMENTATION PAGE

1a. REPORT SECURITY CLASSIFICATION UNCLASSIFIED	1b. RESTRICTIVE MARKINGS
2a. SECURITY CLASSIFICATION AUTHORITY	3. DISTRIBUTION/AVAILABILITY OF REPORT Approved for public release; distribution is unlimited
2b. DECLASSIFICATION/DOWNGRADING SCHEDULE	
4. PERFORMING ORGANIZATION REPORT NUMBER(S) NOSC TR 1294	5. MONITORING ORGANIZATION REPORT NUMBER(S)
6a. NAME OF PERFORMING ORGANIZATION NOSC 6b. OFFICE SYMBOL (if applicable)	7a. NAME OF MONITORING ORGANIZATION
6c. ADDRESS (City, State and ZIP Code) San Diego, CA 92152–5000	7b. ADDRESS (City, State and ZIP Code)
8a. NAME OF FUNDING/SPONSORING ORGANIZATION U.S. Army Cold Regions Research and Engineering Laboratory (CRREL) 8b. OFFICE SYMBOL (if applicable)	9. PROCUREMENT INSTRUMENT IDENTIFICATION NUMBER
8c. ADDRESS (City, State and ZIP Code) Hanover, NH 03755–1290	10. SOURCE OF FUNDING NUMBERS PROGRAM ELEMENT NO. / PROJECT NO. / TASK NO. / AGENCY ACCESSION NO.

11. TITLE (include Security Classification)
Sea and Sky Infrared Radiances Near the Horizon

12. PERSONAL AUTHOR(S)
Herbert G. Hughes

13a. TYPE OF REPORT	13b. TIME COVERED	14. DATE OF REPORT (Year, Month, Day)	15. PAGE COUNT
Final	FROM Apr 1989 TO Jun 1989	June 1989	30

16. SUPPLEMENTARY NOTATION

17. COSATI CODES			18. SUBJECT TERMS (Continue on reverse if necessary and identify by block number)
FIELD	GROUP	SUB-GROUP	infrared backgrounds optical propagation atmospheric physics

19. ABSTRACT (Continue on reverse if necessary and identify by block number)

Atmospheric infrared (8-12-μm) radiances over the ocean were measured from a shore station by using a calibrated thermal imaging system (AGA THERMOVISION, Model 780). The Thermal Video Processor System (THERMOTEKNIX) available with the AGA allowed the mean equivalent blackbody temperatures corresponding to an area 1 degree above and 1 degree below the horizon in the scenes imaged to be determined during different meteorological and surface-wind-speed conditions. For this data set (18 thermograms), the mean sea temperatures differed the most from the mean cloud-free sky temperatures during low wind speed conditions. The differences were found to decrease with increasing wind speed. In contrast, the mean sea and sky temperatures measured during stratus cloud conditions were the same. The cloud-free data are used to evaluate background radiance algorithms, which must be used in the absence of radiometric measurements, to predict the performance of passive surveillance systems operating against airborne targets close to the horizon. Airborne measurements were made of the vertical profiles of meterological parameters and sea surface temperatures determined during 12 of the AGA measurements. From these measurements, LOWTRAN 6 calculations of the mean sky temperatures were found to be in close agreement (correlation coefficient, r = 0.99) with the measured values. Calculated mean sea temperatures (using the Cox–Munk statistical wave slope model with the LOWTRAN code to account for the emissions and sky reflections from the individual wave facets) showed slightly more variations (r = 0.90) than the measurements. These data are also used in a multiple regression analysis to derive an empirical relationship between the apparent mean sea and apparent mean sky temperatures which includes the measured wind speed and actual sea surface temperature.

20. DISTRIBUTION/AVAILABILITY OF ABSTRACT	21. ABSTRACT SECURITY CLASSIFICATION	
☐ UNCLASSIFIED/UNLIMITED ☒ SAME AS RPT ☐ DTIC USERS	UNCLASSIFIED	
22a. NAME OF RESPONSIBLE PERSON Herbert G. Hughes	22b. TELEPHONE (include Area Code) (619) 553–1418	22c. OFFICE SYMBOL Code 543

DD FORM 1473, 84 JAN

83 APR EDITION MAY BE USED UNTIL EXHAUSTED
ALL OTHER EDITIONS ARE OBSOLETE